

# A Wavelet-Based ECG Delineator: Evaluation on Standard Databases

Juan Pablo Martínez\*, Rute Almeida, Salvador Olmos, *Member, IEEE*, Ana Paula Rocha, and Pablo Laguna, *Member, IEEE*

**Abstract**—In this paper, we developed and evaluated a robust single-lead electrocardiogram (ECG) delineation system based on the wavelet transform (WT). In a first step, QRS complexes are detected. Then, each QRS is delineated by detecting and identifying the peaks of the individual waves, as well as the complex onset and end. Finally, the determination of P and T wave peaks, onsets and ends is performed. We evaluated the algorithm on several manually annotated databases, such as MIT-BIH Arrhythmia, QT, European ST-T and CSE databases, developed for validation purposes. The QRS detector obtained a sensitivity of  $Se = 99.66\%$  and a positive predictivity of  $P+ = 99.56\%$  over the first lead of the validation databases (more than 980,000 beats), while for the well-known MIT-BIH Arrhythmia Database,  $Se$  and  $P+$  over 99.8% were attained. As for the delineation of the ECG waves, the mean and standard deviation of the differences between the automatic and manual annotations were computed. The mean error obtained with the WT approach was found not to exceed one sampling interval, while the standard deviations were around the accepted tolerances between expert physicians, outperforming the results of other well known algorithms, especially in determining the end of T wave.

**Index Terms**—ECG wave delineation, P wave, QRS detection, T wave, wavelets.

## I. INTRODUCTION

THE analysis of the ECG is widely used for diagnosing many cardiac diseases, which are the main cause of mortality in developed countries. Since most of the clinically useful information in the ECG is found in the intervals and amplitudes defined by its significant points (characteristic wave peaks and boundaries), the development of accurate and robust methods for automatic ECG delineation is a subject of major importance, especially for the analysis of long recordings. As a matter of fact, QRS detection is necessary to determine the heart rate, and as reference for beat alignment; ECG wave delineation provides fundamental features (amplitudes and intervals) to be used in subsequent automatic analysis.

Manuscript received February 28, 2003; revised August 7, 2003. This work was supported in part by MCyT and FEDER under Project TIC2001-2167-CO2-02, in part by DGA under Project P075/2001, and in part by the integrated action HP2001-0031/CRUP-E26/02. The work of R. Almeida was supported by FCT and ESF (III CSF) under Grant SFRH/BD/5484/2001. *Asterisk indicates corresponding author.*

\*J. P. Martínez is with the Communications Technology Group, Aragon Institute of Engineering Research, University of Zaragoza, María de Luna, 1, 50015 Zaragoza, Spain (e-mail: jpmart@unizar.es).

R. Almeida and A. P. Rocha are with the Departamento de Matemática Aplicada, Faculdade de Ciências, Universidade do Porto, 4169 007 Porto, Portugal.

S. Olmos and P. Laguna are with the Communications Technology Group, Aragon Institute of Engineering Research, University of Zaragoza, 50015 Zaragoza, Spain.

Digital Object Identifier 10.1109/TBME.2003.821031

The topic of automatic delineation of ECG has been widely studied. We can distinguish two main groups of algorithms: QRS detection algorithms and wave delineation algorithms.

The QRS complex is the most characteristic waveform of the ECG signal. Its high amplitude makes QRS detection easier than the other waves. Thus, it is generally used as a reference within the cardiac cycle. A wide diversity of algorithms have been proposed in the literature for QRS detection. An extensive review of the approaches proposed in the last decade can be found in [1]. Older detectors are reviewed in [2]–[4]. A generalized scheme [2] that matches most nonsyntactic QRS detectors presents a two-stage structure: a preprocessing stage, usually including linear filtering followed by a nonlinear transformation, and the decision rule(s).

Concerning delineation (determination of peaks and limits of the individual QRS waves, P and T waves), algorithms usually depart from a previous QRS location and define temporal search windows before and after the QRS fiducial point to seek for the other waves. Once the search window is defined, some technique is applied to enhance the characteristic features of each wave (e.g., its frequency band) in order to find the wave peaks. The localization of wave onsets and ends is much more difficult, as the signal amplitude is low at the wave boundaries and the noise level can be higher than the signal itself. It is also worthwhile to note that there is not any universally acknowledged clear rule to locate the beginning and the end of ECG waves, which complicates the systematization of onset and end localization. One can find in the literature very different delineation approaches based on mathematical models [5]–[7], the signal envelope [8], matched filters [9], ECG slope criteria [10]–[14], second-order derivatives [15], low-pass differentiation (LPD) [16]–[18], the wavelet transform (WT) [19]–[21], nonlinear time-scale decomposition [22], adaptive filtering [23], dynamic time warping [24], artificial neural networks [25], [26], or hidden Markov models [27]. Some of the algorithms presented in these works can only be used to obtain a subset of the ECG characteristic points (e.g., QT interval, QRS limits, T end, etc).

The validation of most recently published QRS detectors is based on standard databases. On the other hand, most of the works about ECG delineation do not use this approach, and that makes the reproducibility and comparability of the performance results more difficult.

The wavelet transform provides a description of the signal in the time-scale domain, allowing the representation of the temporal features of a signal at different resolutions; therefore, it is a suitable tool to analyze the ECG signal, which is characterized by a cyclic occurrence of patterns with different frequency content (QRS complexes, P and T waves). Moreover, the noise and

artifacts affecting the ECG signal also appear at different frequency bands, thus having different contribution at the various scales.

In [19], a multiscale QRS detector including a method for detecting monophasic P and T waves was proposed, although only the QRS detector was validated. In this paper, we present a generalization of that method, including the determination of the individual QRS waves, and a robust delineation of QRS, P, and T waves for a wide range of morphologies. The performance is assessed using standard manually annotated ECG databases, where other algorithms have already been tested: MIT-BIH Arrhythmia [28], QT [29], European ST-T [30], and CSE multi-lead measurement [31] databases. Some of the evaluation results obtained using a preliminary version of this delineator were already presented in [32].

The paper is organized as follows: in Section II, we present the detection and delineation algorithms and the validation process. The results of the validation on several databases and their comparison to other algorithms are given in Section III and discussed in Section IV. Finally, the conclusions are presented in Section V.

## II. MATERIALS AND METHODS

### A. Wavelet Transform

The wavelet transform is a decomposition of the signal as a combination of a set of basis functions, obtained by means of dilation ( $a$ ) and translation ( $b$ ) of a single prototype wavelet  $\psi(t)$ . Thus, the WT of a signal  $x(t)$  is defined as

$$W_a x(b) = \frac{1}{\sqrt{a}} \int_{-\infty}^{+\infty} x(t) \psi\left(\frac{t-b}{a}\right) dt, \quad a > 0. \quad (1)$$

The greater the scale factor  $a$  is, the wider is the basis function and consequently, the corresponding coefficient gives information about lower frequency components of the signal, and vice versa. In this way, the temporal resolution is higher at high frequencies than at low frequencies, achieving the property that the analysis window comprises the same number of periods for any central frequency.

If the prototype wavelet  $\psi(t)$  is the derivative of a smoothing function  $\theta(t)$ , it can be shown [33], [34] that the wavelet transform of a signal  $x(t)$  at scale  $a$  is

$$W_a x(b) = -a \left(\frac{d}{db}\right) \int_{-\infty}^{+\infty} x(t) \theta_a(t-b) dt \quad (2)$$

where  $\theta_a(t) = (1/\sqrt{a})\theta(t/a)$  is the scaled version of the smoothing function. The wavelet transform at scale  $a$  is proportional to the derivative of the filtered version of the signal with a smoothing impulse response at scale  $a$ . Therefore, the zero-crossings of the WT correspond to the local maxima or minima of the smoothed signal at different scales, and the maximum absolute values of the wavelet transform are associated with maximum slopes in the filtered signal.

Regarding our application, we are interested in detecting ECG waves, which are composed of slopes and local maxima (or minima) at different scales, occurring at different time instants within the cardiac cycle. Hence, the convenience of using such a type of prototype wavelet.

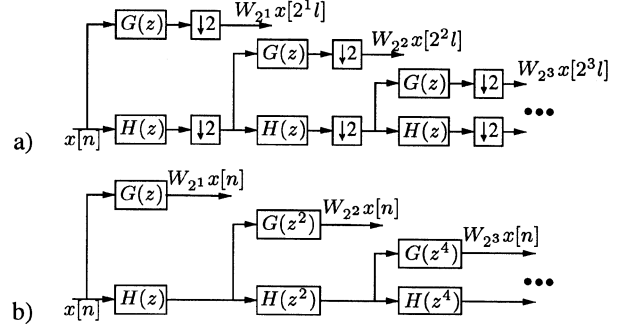


Fig. 1. Two filter-bank implementations of DWT. (a) Mallat's algorithm. (b) Implementation without decimation (*algorithme à trous*).

The scale factor  $a$  and/or the translation parameter  $b$  can be discretized. The usual choice is to follow a dyadic grid on the time-scale plane:  $a = 2^k$  and  $b = 2^k l$ . The transform is then called *dyadic wavelet transform*, with basis functions

$$\psi_{k,l}(t) = 2^{-k/2} \psi(2^{-k}t - l); \quad k, l \in \mathbb{Z}^+. \quad (3)$$

For discrete-time signals, the dyadic discrete wavelet transform (DWT) is equivalent, according to Mallat's algorithm, to an octave filter bank [35], and can be implemented as a cascade of identical cells [low-pass and high-pass finite impulse response (FIR) filters], as illustrated in Fig. 1(a). From the transformed coefficients  $W_{2^k}x[2^k l]$  and the low-pass residual, the original signal can be rebuilt using a reconstruction filter bank. However, for this application we are only interested in the analysis filter bank.

The downsamplers after each filter in Fig. 1(a) remove the redundancy of the signal representation. As side effects, they make the signal representation time-variant, and reduce the temporal resolution of the wavelet coefficients for increasing scales. To keep the time-invariance and the temporal resolution at different scales, we use the same sampling rate in all scales, what is achieved by removing the decimation stages and interpolating the filter impulse responses of the previous scale. This algorithm, called *algorithme à trous* [36], is shown in Fig. 1(b). Using this algorithm, the equivalent frequency response for the  $k$ th scale is

$$Q_k(e^{j\omega}) = \begin{cases} G(e^{j\omega}), & k = 1 \\ G(e^{j2^{k-1}\omega}), \prod_{l=0}^{k-2} H(e^{j2^l\omega}) & k \geq 2 \end{cases}. \quad (4)$$

### B. Prototype Wavelet Used in This Paper

In this paper, we used as prototype wavelet  $\psi(t)$  a quadratic spline originally proposed in [33]. This wavelet was already applied to ECG signals in [19] and [21], while in [20], the derivative of a Gaussian smoothing function was used. The quadratic spline Fourier transform is

$$\Psi(\Omega) = j\Omega \left(\frac{\sin(\frac{\Omega}{4})}{\frac{\Omega}{4}}\right)^4. \quad (5)$$

From (5), the wavelet can be easily identified as the derivative of the convolution of four rectangular pulses, i.e., the derivative of a low-pass function. Fig. 2 represents the wavelet and smoothing functions used in this paper.

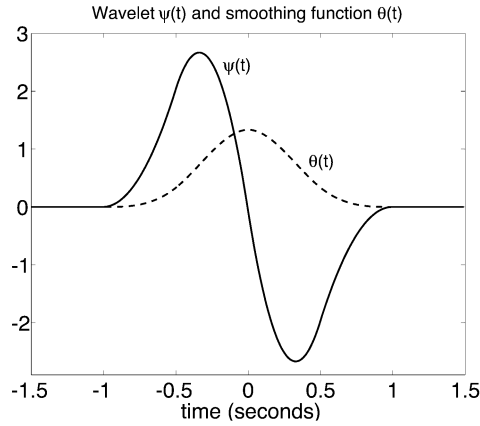


Fig. 2. Prototype wavelet  $\psi(t)$  and smoothing function  $\theta(t)$ .

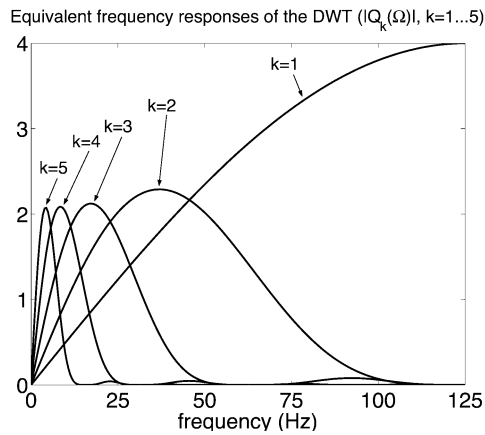


Fig. 3. Equivalent frequency responses of the DWT at scales  $2^k$ ,  $k = 1, \dots, 5$  for 250-Hz sampling rate.

For the selected prototype wavelet, the filters  $H(z)$  and  $G(z)$  to implement the DWT as in Fig. 1 are [19], [37]

$$\begin{aligned} H(e^{j\omega}) &= e^{j\omega/2} \left( \cos \frac{\omega}{2} \right)^3 \\ G(e^{j\omega}) &= 4j e^{j\omega/2} \left( \sin \frac{\omega}{2} \right), \end{aligned} \quad (6)$$

which are FIR filters with impulse responses

$$\begin{aligned} h[n] &= \frac{1}{8} \cdot \{\delta[n+2] + 3\delta[n+1] + 3\delta[n] + \delta[n-1]\} \\ g[n] &= 2 \cdot \{\delta[n+1] - \delta[n]\}. \end{aligned} \quad (7)$$

Using the *algorithme à trous* of Fig. 1(b) and (4) and (6), the frequency responses of the first five scales are those represented in Fig. 3, considering a sampling frequency of 250 Hz. It is noteworthy that the transfer functions show a low-pass differentiator characteristic. As the analysis filters have linear phase [19], the outputs of the filters can be realigned in order to present the same delay with respect to the original ECG. Therefore, the wavelet-based approach for ECG delineation can be considered as a differentiator filter-bank approach with the filter responses in (4).

### C. Adaptation of the Filters to Other Sampling Frequencies

The result of using the same filters for a sampling rate other than 250 Hz is the frequency-scaling of the bands in Fig. 3. Thus,

some adaptation procedures are required for the system to be able to handle equivalently ECG signals with different sampling frequencies. Other previously published waveform delineators using the WT [19]–[21] have not accounted for this fact, considering a unique sampling frequency ( $f_s = 250$  Hz).

Resampling the signal is a time-demanding solution. A better solution is to compute, for each  $f_s$ , a new set of filters having equivalent *analogue* frequency responses as close as possible to the ones of Fig. 3. For this purpose, we resampled adequately the equivalent filter impulse responses at 250 Hz  $q_k^{250}[n] = \mathfrak{F}^{-1} \{Q_k(e^{j\omega})\}$  (where  $\mathfrak{F}$  stands for the Fourier transform) to other sampling rates. The equivalent frequency responses corresponding to the sampling rates of MIT-BIH Arrhythmia and CSE databases (360 Hz and 500 Hz, respectively) are shown and compared with the ones at 250 Hz in Fig. 4. It can be observed that the frequency responses of the adapted filter bank constitute a good approximation of the original filters up to a frequency of 45–50 Hz.

### D. Description of the Algorithms

The algorithms presented in this section apply directly over the digitized ECG signal without any prefiltering. The ECG signal can, in any case, be preprocessed as usual in order to reduce the noise level. Nevertheless, frequency domain filtering is implicitly performed when computing the DWT, making the system robust and allowing the direct application over the raw ECG signal.

From the equivalent responses in Fig. 3 and according to the spectrum of the ECG signal waves [38], it is clear that most of the energy of the ECG signal lies within the scales  $2^1$  to  $2^5$ . For scales higher than  $2^4$ , the energy of the QRS is very low. The P and T waves have significant components at scale  $2^5$  although the influence of baseline wandering is important at this scale.

Fig. 5, inspired by [19, Fig. 1], shows several simulated waves similar to those in the ECG, together with the first five scales of their DWT. As exemplified by (a), monophasic waves produce a positive maximum-negative minimum pair along the scales, with a zero crossing between them. Each sharp change in the signal is associated to a line of maxima or minima across the scales. In wave (b), which simulates a QRS complex, it can be observed that the small Q and S wave peaks have zero crossings associated in the WT, mainly at scales  $2^1$  and  $2^2$ . P or T-like waves (c) have their major component at scales  $2^4$  to  $2^5$ , whereas artifacts like (d) produce isolated maximum or minimum lines which can be easily discarded. If the signal is contaminated with high-frequency noise (e), the most affected scales are  $2^1$  and  $2^2$ , being higher scales essentially immune to this sort of noise. Baseline wander (f) affects only at scales higher than  $2^4$ .

Using the information of local maxima, minima and zero crossings at different scales, the algorithm identifies the significant points in the following four steps: 1) detection of QRS complexes; 2) detection and identification of the QRS individual waves (Q, R, S, R'), and determination of the QRS complex boundaries; 3) T wave detection and delineation; and 4) P wave detection and delineation.

1) *QRS Detection*: First of all, QRS complexes are detected using an algorithm based on the multiscale approach proposed by Li and coworkers in [19]. This algorithm searches across the scales for “maximum modulus lines” exceeding some

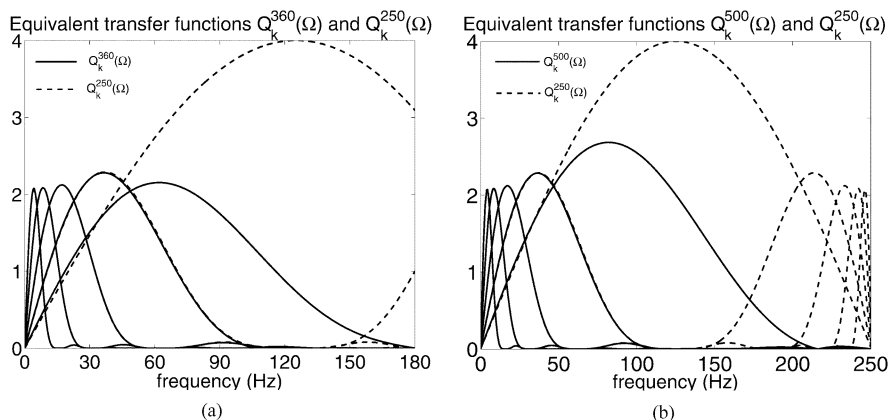


Fig. 4. Equivalent frequency responses of the filters used for sampling rates of (a) 360 Hz and (b) 500 Hz (continuous lines). Dashed lines are the equivalent frequency responses of the original filters for signals sampled at 250 Hz.

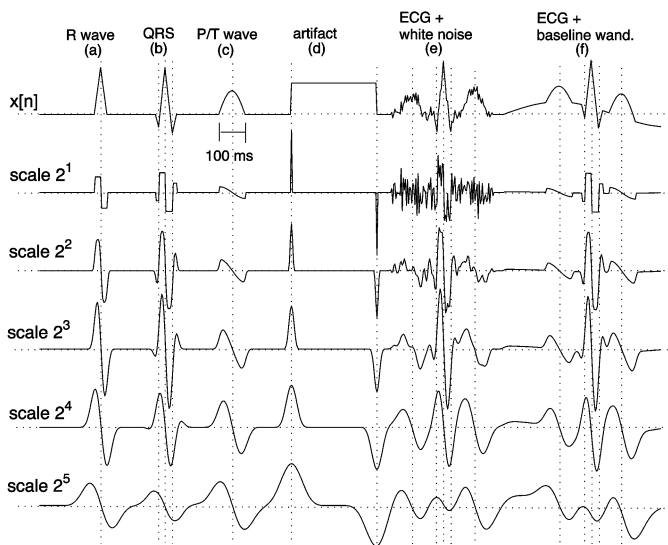


Fig. 5. WT at the first five scales of ECG-like simulated waves. (Inspired by [19, Fig. 1].).

thresholds at scales from  $2^1$  to  $2^4$ ; namely,  $\epsilon_{QRS}^1$ ,  $\epsilon_{QRS}^2$ ,  $\epsilon_{QRS}^3$ , and  $\epsilon_{QRS}^4$  (see Appendix for more details about the thresholds). After rejecting all isolated and redundant maximum lines, the zero crossing of the WT at scale  $2^1$  between a positive maximum-negative minimum pair is marked as a QRS. Other protection measures are taken, like a refractory period or a search back with lowered thresholds if a significant time has elapsed without detecting any QRS. Our implementation, though based on [19] is slightly different: the search for the main wave of the QRS is not restricted to an R wave, allowing the detection of negative waves (negative minimum – positive maximum pairs). Afterwards, the individual waves are identified. Besides, our algorithm does not include regularity analysis, but only amplitude based criteria, and the thresholds are not updated for each beat, but for each excerpt of  $2^{16}$  samples.

In Fig. 6, some ECG excerpts from the MIT-BIH Arrhythmia database have been selected to illustrate the robustness of the detector dealing with motion artifacts, muscular noise, baseline wandering, and changes in the QRS morphology.

2) *QRS Delineation (Onset, End and Individual Waves)*: One of the novelties with respect to [19] is the

detection and identification of the QRS individual waves. The algorithm departs from the position given by the detector,  $n_{QRS}$ , which must be flanked by a pair of maximum moduli with opposite signs at scale  $2^2$ , namely at  $n_{pre}$  and  $n_{post}$ . The delineator looks before  $n_{pre}$  and after  $n_{post}$  for significant maxima of  $|W_{2^2}x[n]|$  accounting for other adjacent slopes within the QRS complex. To consider a local maximum modulus as significant, it must exceed the threshold,  $\gamma_{QRS_{pre}}$  or  $\gamma_{QRS_{post}}$  respectively for previous or subsequent waves. The zero crossings between these significant slopes at scale  $2^1$  are assigned to wave peaks, and labeled depending on the sign and the sequence of the maximum moduli. The algorithm considers any possible QRS morphology with three or less waves (QRS, RSR', QR, RS, R, and QS complexes), and includes protection measures, based on time interval and sign rules, to reject notches in waves and anomalous deflections in the ECG signal. See Fig. 7 for examples of these complexes.

The onset (end) of the QRS is before (after) the first (last) significant slope of the QRS, which is associated with a maximum of  $|W_{2^k}x[n]|$ . So, we first identify the samples of the first and last peaks associated with the QRS in  $W_{2^2}x[n]$ , say  $n_{first}$  and  $n_{last}$ . Then, candidates to onset and end are determined by applying two criteria: i) searching for the sample where  $|W_{2^2}x[n]|$  is below a threshold ( $\xi_{QRS_{on}}$  or  $\xi_{QRS_{end}}$ ) relative to the amplitude of the maximum modulus ( $|W_{2^2}x[n_{first}]|$  or  $|W_{2^2}x[n_{last}]|$ ); ii) searching for a local minimum of  $|W_{2^2}x[n]|$  before  $n_{first}$  or after  $n_{last}$ . Finally the QRS onset and end are selected as the candidates that supply the nearest sample to the QRS.

3) *T Wave Detection and Delineation*: The process for multiscale T wave detection and delineation is as follows: first of all, we define a search window for each beat, relative to the QRS position and depending on a recursively computed RR interval. Within this window, we look for local maxima of  $|W_{2^4}x[n]|$ . If at least two of them exceed the threshold  $\epsilon_T$ , a T wave is considered to be present. In this case, the local maxima of WT with amplitude greater than  $\gamma_T$  are considered as significant slopes of the wave, and the zero crossings between them as the wave peaks. Depending on the number and polarity of the found maxima, we assign one out of six possible T wave morphologies: positive (+), negative (-), biphasic (+/- or -/+), only upwards, and only downwards (see Fig. 8). If the T wave is not found in scale  $2^4$  we repeat the above process over  $|W_{2^5}x[n]|$ . Attending to the loss of time resolution in the growing scales,

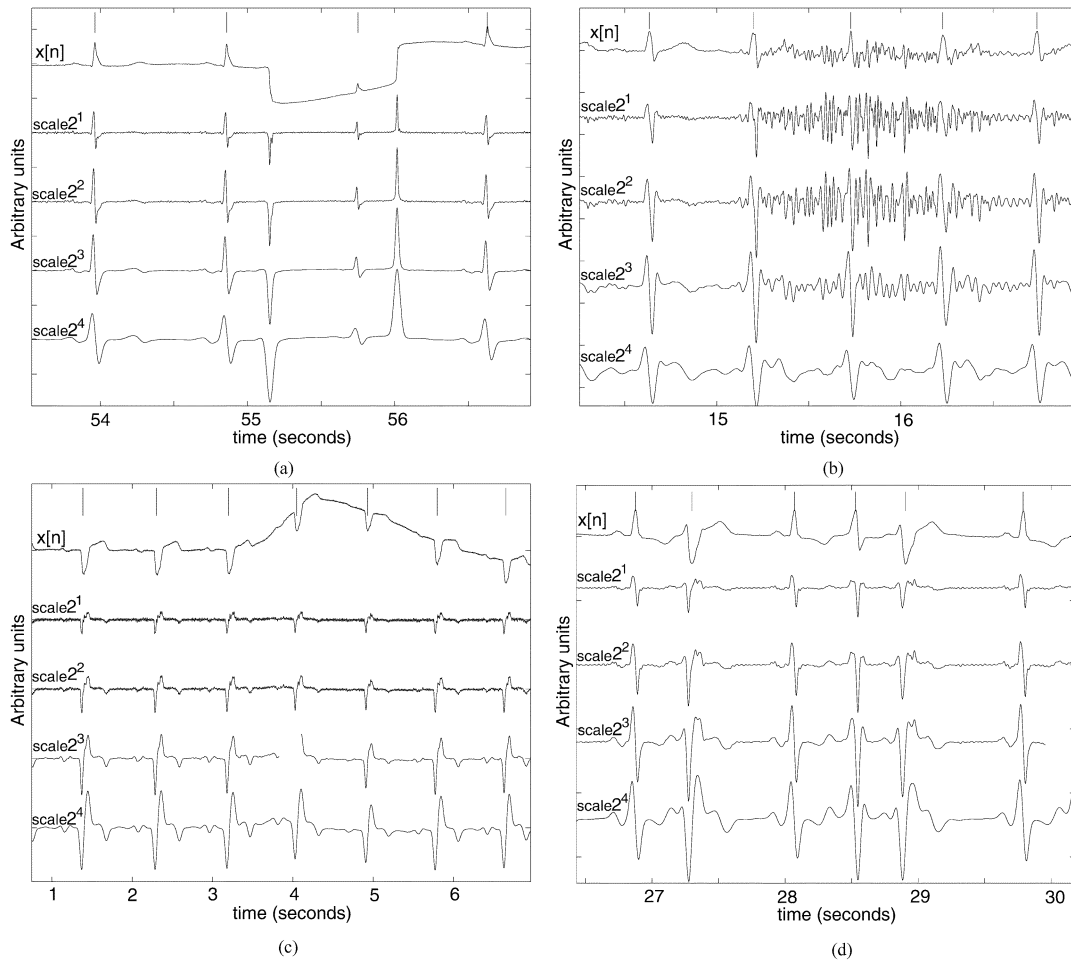


Fig. 6. Examples of the behavior of the QRS detector dealing with different kinds of noise and morphology changes. (a) Motion artifact, (b) muscular noise, (c) baseline wandering, and (d) QRS morphology changes. The ECG signal, the WT's first four scales and the detected QRS complexes (vertical lines) are shown in each panel.

the peak(s) of the T wave correspond to the zero crossing(s) at scale  $2^3$ , if they exist, or at the scale  $2^k$  in which T wave was found. To identify the wave limits, we used the same criteria as for QRS onset and end, with thresholds  $\xi_{Ton}$  and  $\xi_{Tend}$  applied to scale  $2^k$ .

4) *P Wave Detection and Delineation*: The P wave algorithm is similar to the T wave algorithm, using an appropriate RR-dependent search window and adequate thresholds ( $\epsilon_P$ ,  $\gamma_P$ ,  $\xi_{Pon}$  and  $\xi_{Pend}$ ). For P wave only four different morphologies are admitted: positive (+), negative (-), and biphasic (+/-, -/+), as illustrated in Fig. 9.

### E. Validation

As there is no *golden rule* to determine the peak, onset and end of the ECG waves, the validation of the delineator must be done using manually annotated databases. For these purposes, we used some easily-available or standard databases, namely the MIT-BIH Arrhythmia database (MITDB), the QT database (QTDB), the European ST-T database (EDB) and the data set 3 of the CSE multilead measurement database (CSEDB). The main characteristics of these databases are compiled in Table I.

The MITDB includes specially selected Holter recordings with anomalous but clinically important phenomena. The EDB files present ischemic episodes extracted from Holter recordings. These databases include annotations of QRS positions: R

marks (MITDB) or QRS onsets (EDB). The QTDB includes some records from EDB and MITDB and also from several other MIT-BIH databases (ST Change, Supraventricular Arrhythmia, Normal Sinus Rhythm, Sudden Death, and Long Term). This database was developed for wave limits validation purposes and it provides cardiologist annotations for at least 30 beats per recording (ref1), with marks including QRS complexes, P and T waves peaks, onsets and ends. That makes an amount of more than 3600 annotated beats. The QTDB also includes, for 11 out of its 105 records, an additional annotation performed by a second cardiologist (ref2), making a total of 404 beats with a double reference annotation. In 79 of the 105 recordings additional annotation files are provided with the QRS positions manually annotated or audited during the whole recording. The CSEDB signals include the 12 standard leads and the Frank leads. This database supplies, in a limited number of beats (at most one beat per record), *median referee* annotations based on five referee cardiologists. The cardiologists only analyzed a subsample of the library (every fifth record) and, additionally some waves for which a set of analysis programs differed significantly. Thus, the number of manually annotated beats is scarce (32 beats).

For validation of QRS detection, we used the MITDB, the EDB, and the QTDB (79 records) and to evaluate the delineation performance, we used the whole QTDB and the CSEDB.

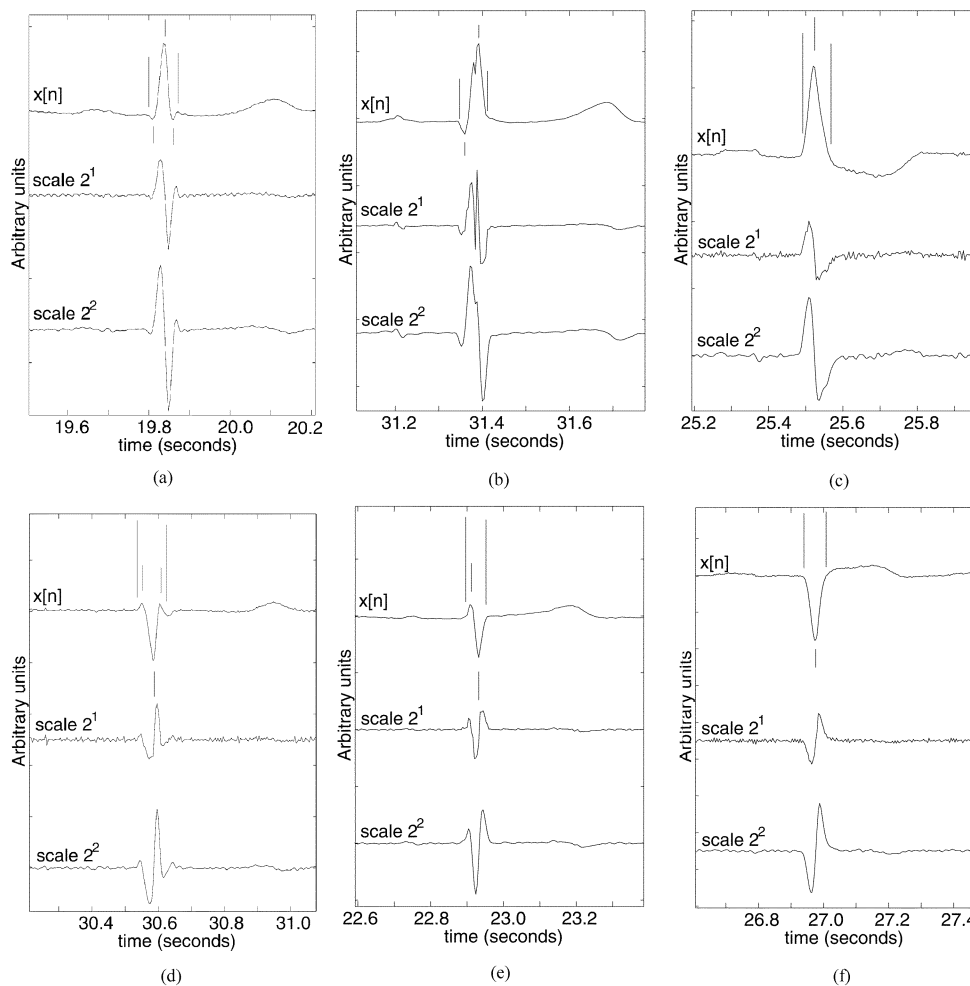


Fig. 7. Examples of beats from the QTDB with different QRS complex morphologies with their WT at scales  $2^1$  and  $2^2$  and the peaks (short lines) and QRS boundaries (long lines) determined by the algorithm. (a) QRS complex, (b) QRS complex (with notch), (c) R complex, (d) RSR' complex (e), RS complex, and (f) QS complex.

These are, to our knowledge, the only two standard databases that have been used to test delineation techniques. Additionally, EDB database was also used for performance evaluation of the QRS onset determination.

For QRS detection, only the first channel of each record was processed with the aim of comparing with other published works. The wavelet-based delineator works on a single-channel basis, while the manual annotation process was performed having in sight all available leads. Therefore, to compare in a reasonable way the manual annotations on the QTDB and EDB with the two single-channel annotation sets produced by the delineator, we chose for each point the channel with less error. In the CSEDB we obtained with our system 15 different sets of annotations, one for each channel, and we needed a more complex rule for selecting a single location for each characteristic point. We used for that purpose a rule consisting of ordering the 15 single-lead annotations and selecting as the onset (end) of a wave the first (last) annotation whose  $k$  nearest neighbors lay within a  $\delta$  ms interval. This rule had been already used in [11] ( $k = 2$  and  $\delta = 6$  ms for QRS boundaries) and [16] ( $k = 3$ , and  $\delta = 6$  ms for P wave limits and QRS onset,  $\delta = 10$  ms for QRS end, and  $\delta = 12$  ms for T end).

To assess the QRS detector we calculated the sensitivity  $Se = TP/(TP + FN)$  and positive predictivity  $P^+ = TP/(TP + FP)$ , where TP is the number of true positive detections, FN stands for the number of false negative detections, and FP stands for the number of false positive misdetections. Regarding wave delineation, we calculated  $m$  as the average of the errors, taken as the time differences between automatic and cardiologist annotations. The average standard deviation ( $s$ ) of the error was computed by averaging the intrarecording standard deviations. In the CSEDB, as there is only one annotated beat per record,  $s$  corresponds to the standard deviation of the errors. For QTDB,  $Se$  was also calculated, but given the format of this database, it was not possible to quantify the  $P^+$ , as it was already noted in [7]. As a matter of fact, when there is not an annotation, we do not know either if the cardiologist considered that no wave was present or if he simply believed that he could not confidently annotate the point (e.g., because of the noise). Anyway, for points other than the QRS complex,  $P^+$  can be calculated considering each absent reference mark on an annotated beat as a not present wave decision. The obtained values can be interpreted as a lower limit ( $P_{\min}^+$ ) for the actual  $P^+$ .

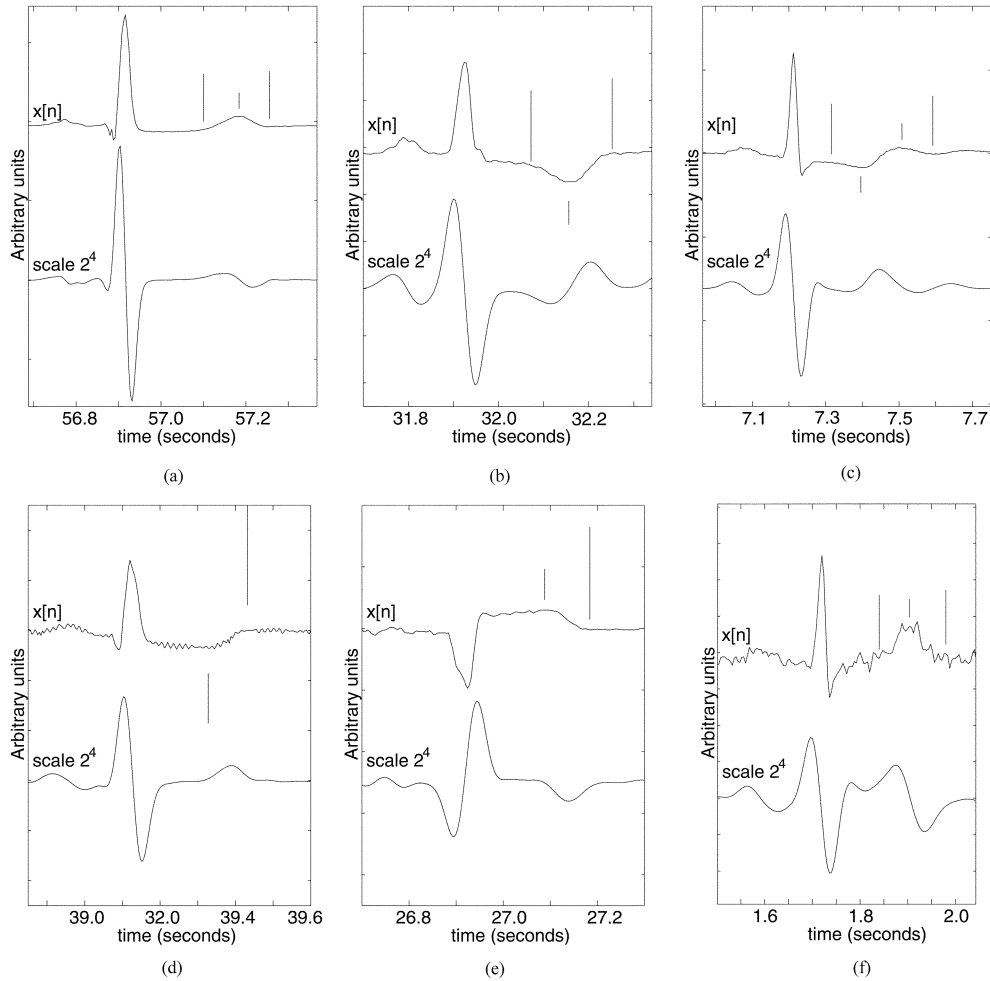


Fig. 8. Examples of different T wave morphologies, and their wavelet transform at scale  $2^4$ . Short vertical lines show peak annotations while long lines denote wave boundaries. (a) Positive T wave, (b) negative T wave, (c) biphasic T wave, (d) ascending T wave, (e) descending T wave, and (f) T wave with low SNR.

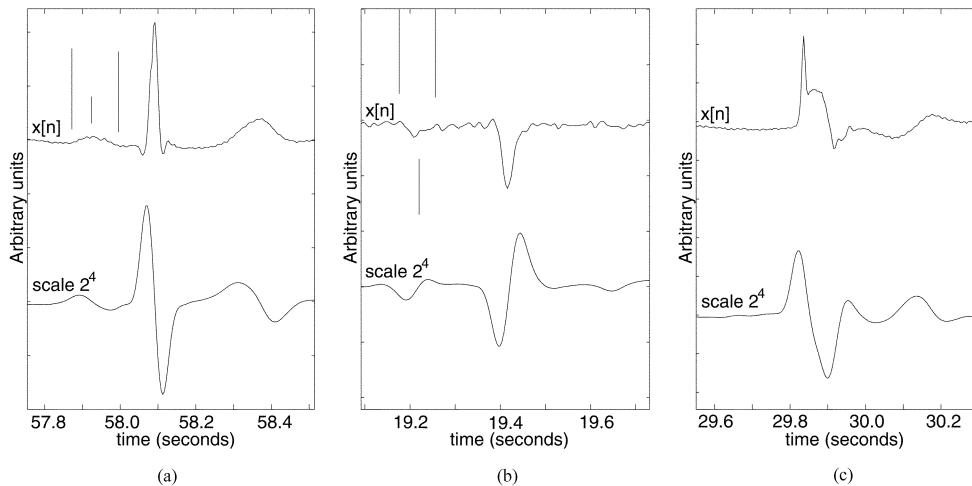


Fig. 9. Examples of P waves with different polarities and in absence of P wave, their WT at scale  $2^4$ , and marks for peaks, onsets and ends. (a) Positive P wave, (b) negative P wave, and (c) absent P wave.

### III. RESULTS

#### A. Results for QRS Detection

The detection performance on the MITDB, QTDB, and EDB obtained by our WT-based QRS detector, the software Aristotle

[39] (in single-channel mode), and other published detectors are given in Table II. Most of the algorithms were tested on the MITDB. In some works [20], [40], the first 5 min of the MITDB were used as a learning period, and were not considered in the validation. Since our algorithm does not need any learning pe-

TABLE I  
CHARACTERISTICS OF THE VALIDATION DATABASES

| Database | files | leads | $f_s$ (Hz) | resol.         | rec. duration |
|----------|-------|-------|------------|----------------|---------------|
| MITDB    | 48    | 2     | 360        | $5\mu\text{V}$ | 30 minutes    |
| QTDB     | 105   | 2     | 250        | $5\mu\text{V}$ | 15 minutes    |
| EDB      | 90    | 2     | 250        | $5\mu\text{V}$ | 120 minutes   |
| CSEDB    | 125   | 15    | 500        | $1\mu\text{V}$ | 10 seconds    |

riod, the entire recordings were considered. We excluded segments with ventricular flutter in record 207 of MITDB (2 min 24 s) and those annotated as *unreadable* in the EDB (57 min 6 s in lead 1, and only 2 min 46 s in both leads simultaneously).

Partial results are presented in [20] using the first channel of the eight first recordings of the MITDB (100 to 107) and leaving out the first 5 min. That WT-based QRS detector achieve in those recordings 93 FP and 84 FN out of 14 481 analyzed beats ( $Se = 99.42\%$  and  $P^+ = 99.36\%$ ). Our WT-based detector presented in those excerpts 43 FP and 23 FN ( $Se = 99.84\%$  and  $P^+ = 99.70\%$ ).

### B. Delineation Results

The global validation results obtained with the WT-based delineator (this paper) and a low-pass-differentiator-based method (LPD) [16] on the QTDB are given in Table III. A previous version of the LPD algorithm had already been validated on the QTDB in [47]. The results for T peak and T end of the recently proposed T-U complex detector in [7] are shown as well in that table. In the last row, we include the accepted *two-standard-deviation* tolerances given by the CSE working party from measurements made by different experts [48, Table 2].

In Table IV we compare, within the subset of the QTDB with double reference annotations, the delineation errors with respect to both referees (ref1 and ref2) and the intercardiologist differences. Since the second cardiologist did not annotate any P wave, no results are given for this wave.

The special interest in T wave delineation and the high difficulty of the determination of its end justifies a more detailed study. A record-by-record classification was performed as proposed in [47] and more recently in [7]. In order to facilitate the comparison with previous works we chose the same threshold than in [7], i.e., 15 ms for the bias and 30.6 ms for the standard deviation. Thus, the records are classified into four groups, according to: Group I: bias < 15 ms and  $s < 30.6$  ms; Group II: bias > 15 ms and  $s < 30.6$  ms; Group III: bias < 15 ms and  $s > 30.6$  ms and Group IV: bias > 15 ms and  $s > 30.6$  ms. The stratification results with the three algorithms for the T wave peak and T end are given in Table V.

In the CSEDB, we used the rule explained in Section II-E for selecting a single multilead position for each significant point. The performance was found to be very sensitive to the chosen  $k$  and  $\delta$  values. We obtained the best performance using  $k = 3$  and  $\delta = 4$  ms for P limits, 10 ms for QRS end, and 12 ms for QRS onset and T end. The multilead performance results, taking as reference the *median cardiologist* annotations are given in Table VI.

Finally, we also used the EDB for QRS onset validation, considering that the QRS reference points annotated in this database are QRS onset marks. Selecting the channel with less error for each beat, we obtained a mean error of 0.1 ms and an averaged standard deviation of 7.5 ms over 790 287 beats.

## IV. DISCUSSION

The proposed WT-based delineation system achieves very good detection performance on the studied databases. The QRS detector attains  $Se = 99.66\%$  and  $P^+ = 99.56$  (0.78% of errors) on the first lead of the three databases: 983 423 beats (> 220 hours of ECG). On the MITDB (widely used to evaluate QRS detectors), only three detectors based on WT ([19], [21] and this paper) and a very recent one based on more classical approaches [46], report  $Se$  and  $P^+$  over 99.8%. However, the extensive use of the MITDB as a testing database can hide an overtuning of the detector parameters to fit this particular database. Consequently, the validation of the same detector on a second data set without any later *parameter tuning* can help to obtain more reliable performance results. Actually, we fixed the thresholds using signals of the MITDB as training set, but as it can be observed in Table II, we obtained similar performance on the QTDB or the EDB, modifying only the resampling of the filters as explained in Section II-C to cope with the differences in the sampling frequency. It is important to remark that in EDB, the first channel of record e0305 (which exhibits very narrow and tall T waves) is responsible for 42% of the FP and 57% of the FN. Excluding this record, the performance in the EDB is  $Se = 99.84\%$ ,  $P^+ = 99.70\%$  and the total performance in the three datasets increases to  $Se = 99.84\%$ ,  $P^+ = 99.73\%$  over 974 042 beats.

The WT-based detector, in contrast to most QRS detectors found in the literature, allows to take advantage of the same wavelet analysis stage for ECG wave delineation, due to the particularly appropriate characteristics of time-scale analysis. In [19] and [21], the possibility of detecting monophasic P and T wave peaks was stated, but not evaluated. Only in [20], an algorithm for detecting the peaks, onsets and ends of monophasic P and T waves was validated using the CSEDB. Our algorithm allows delineation of a wide variety of QRS complex, P wave and T wave morphologies.

The delineation performance on the QTDB (Table III) shows that our WT algorithm can detect with high sensitivity the P and T waves annotated by cardiologists in the ECG ( $Se = 98.87\%$  for the P waves and  $99.77\%$  for the T waves), and can delineate them with mean errors which are in all cases smaller than or around one sample (4 ms). The standard deviations are around three samples for the P wave, two samples for QRS onsets and ends, and three to four samples for the T peak and the T end. Despite  $P_{\min}^+$  is a conservative estimate of the actual  $P^+$ , the values found are also satisfactory ( $P_{\min}^+ = 91.0\%$  for the P waves and  $P_{\min}^+ = 97.8\%$  for the T waves).

The comparison of our results with those of the LPD approach and the TU detector allows to observe that our algorithm outperforms the others clearly in the T wave delineation, especially in the T wave end, where the standard deviation of the error is nearly reduced in one third. The results in the other points are quite similar and the differences between them are small in comparison to the sampling interval.

Some works considered the values given by the CSE Working Party in [48, Table 2] as a reference for delineation error tolerances. In the cited article, it was stated “the standard deviation of the differences [of a program results] from the reference should not exceed certain limits as listed in Table II”. However, the

TABLE II  
QRS DETECTION PERFORMANCE COMPARISON ON SEVERAL DATABASES (FIRST CHANNEL). (N/R: NOT REPORTED)

| Database | QRS detector             | # annotations | TP     | FP    | FN    | %error | Se %  | P+ %  |
|----------|--------------------------|---------------|--------|-------|-------|--------|-------|-------|
| MITDB    | WT (this work)           | 109428        | 109208 | 153   | 220   | 0.34   | 99.80 | 99.86 |
|          | Aristotle [39]           | 109428        | 107567 | 94    | 1861  | 1.79   | 98.30 | 99.91 |
|          | Li et al. (WT) [19]      | 104182*       | 104070 | 65    | 112   | 0.17   | 99.89 | 99.94 |
|          | Afonso et al. [40]       | 90909         | 90535  | 406   | 374   | 0.86   | 99.59 | 99.56 |
|          | Bahoura et al. (WT) [21] | 109809*       | 109635 | 135*  | 184*  | 0.29   | 99.83 | 99.88 |
|          | Lee et al. [41]          | 109481        | 109146 | 137   | 335   | 0.43   | 99.69 | 99.88 |
|          | Hamilton et al. [42]     | 109267        | 108927 | 248   | 340   | 0.54   | 99.69 | 99.77 |
|          | Pan et al. [43]          | 109809*       | 109532 | 507   | 277   | 0.71   | 99.75 | 99.54 |
|          | Poli et al. [44]         | 109963        | 109522 | 545   | 441   | 0.90   | 99.60 | 99.50 |
|          | Moraes et al. [45]       | N/R           | N/R    | N/R   | N/R   | N/R    | 99.22 | 99.73 |
|          | Hamilton [46]            | N/R           | N/R    | N/R   | N/R   | 99.80  | 99.80 |       |
| QTDB     | WT (this work)           | 86892         | 86824  | 107   | 68    | 0.20   | 99.92 | 99.88 |
|          | ARISTOTLE [39]           | 86892         | 84458  | 459   | 2434  | 3.33   | 97.20 | 99.46 |
| EDB      | WT (this work)           | 787103        | 784059 | 4077  | 3044  | 0.90   | 99.61 | 99.48 |
|          | ARISTOTLE [39]           | 787103        | 748468 | 10405 | 38635 | 6.23   | 95.09 | 98.63 |

\* Values computed according to the record-by-record tables in the referred works since there is a discrepancy between total values and the sum of the individual ones.

TABLE III  
DELINEATION PERFORMANCE COMPARISON IN THE QTDB (TWO-CHANNELS). (N/R: NOT REPORTED, N/A: NOT APPLICABLE)

| Method                                    | Parameters                        | P <sub>on</sub> | P <sub>peak</sub> | P <sub>end</sub> | QRS <sub>on</sub> | QRS <sub>end</sub> | T <sub>peak</sub> | T <sub>end</sub> |
|---|-----------------------------------|-----------------|-------------------|------------------|-------------------|--------------------|-------------------|------------------|
|   | # annotations                     | 3194            | 3194              | 3194             | 3623              | 3623               | 3542              | 3542             |
| WT<br>(this work)                         | Se (%)                            | 98.87           | 98.87             | 98.75            | 99.97             | 99.97              | 99.77             | 99.77            |
|   | P <sub>min</sub> <sup>+</sup> (%) | 91.03           | 91.03             | 91.03            | N/A               | N/A                | 97.79             | 97.79            |
|   | m±s (ms)                          | 2.0±14.8        | 3.6±13.2          | 1.9±12.8         | 4.6±7.7           | 0.8±8.7            | 0.2±13.9          | -1.6±18.1        |
| LPD                                       | Se (%)                            | 97.7            | 97.7              | 97.7             | 99.92             | 99.92              | 99.0              | 99.0             |
|   | P <sub>min</sub> <sup>+</sup> (%) | 91.17           | 91.17             | 91.17            | N/A               | N/A                | 97.74             | 97.71            |
|   | m±s (ms)                          | 14.0±13.3       | 4.8±10.6          | -0.1±12.3        | -3.6±8.6          | -1.1±8.3           | -7.2±14.3         | 13.5±27.0        |
| TU [7]                                    | Se (%)                            | N/A             | N/A               | N/A              | N/A               | N/A                | 92.6              | 92.6             |
|   | P <sub>min</sub> <sup>+</sup> (%) | N/A             | N/A               | N/A              | N/A               | N/A                | N/R               | N/R              |
|   | m±s (ms)                          | N/A             | N/A               | N/A              | N/A               | N/A                | -12.0±23.4        | 0.8±30.3         |
| <b>Tolerances (2s<sub>CSE</sub>) [48]</b> |                                   | <b>10.2</b>     | -                 | <b>12.7</b>      | <b>6.5</b>        | <b>11.6</b>        | -                 | <b>30.6</b>      |

TABLE IV  
DELINEATION PERFORMANCE COMPARISON BETWEEN THE PRESENTED DELINEATOR AND BOTH REFEREES

| validation             | QRS <sub>on</sub><br>m±s (ms) | QRS <sub>off</sub><br>m±s (ms) | T <sub>peak</sub><br>m±s (ms) | T <sub>off</sub><br>m±s (ms) |
|------------------------|-------------------------------|--------------------------------|-------------------------------|------------------------------|
| WT vs ref1 (all rec.)  | 4.6±7.7                       | 0.8±8.7                        | 0.2±13.9                      | -1.6±18.1                    |
| WT vs ref1 (11 rec.)   | 5.7±10.3                      | 0.8±10.3                       | -0.6±8.9                      | -9.7±18.1                    |
| WT vs ref2 (11 rec.)   | 4.75±9.1                      | 0.8±6.5                        | 0.3±12.5                      | -10.8±20.0                   |
| ref2 vs ref1 (11 rec.) | 5.3±11.1                      | -0.1±12.2                      | 5.1±15.9                      | 2.1±22.4                     |

limits given in that table, were obtained as two standard deviations of the differences (in milliseconds) between the median of the individual readers and the final referee estimates. As a consequence, some authors [7], [16], [20], [24] considered that an algorithm should accomplish  $s < 2s_{CSE}$  (loose criterion), while for others [11], [22], a standard deviation  $s < s_{CSE}$  should be attained (strict criterion). From the results in the QTDB, WT and LPD detectors would accomplish the “loose criteria” in P end, QRS end, and T end, and nearly for QRS onset. The “strict criteria” would not be accomplished by any of the mentioned

algorithms, although the tolerance for T end would be nearly accomplished by the WT approach.

However, the interpretation of the CSE tolerances when assessing the results on the QTDB is not so simple, since they were computed from a set of signals with different number of channels, resolution, sampling frequency, quality, and rhythms. Given the 11 recordings annotated by a second cardiologist in the QTDB, we could get an estimate of the intercardiologist differences in this database. It can be seen from Table IV that the error between the WT-based delineation system and each of the

TABLE V  
QTDB RECORDING STRATIFICATION ACCORDING TO DELINEATION ACCURACY

| Method | $T_{peak}$ |                |          |                |           |                |          |                | $T_{end}$ |                |          |                |           |                |          |                |
|--------|------------|----------------|----------|----------------|-----------|----------------|----------|----------------|-----------|----------------|----------|----------------|-----------|----------------|----------|----------------|
|        | Group I    |                | Group II |                | Group III |                | Group IV |                | Group I   |                | Group II |                | Group III |                | Group IV |                |
|        | %          | $m \pm s$ (ms) | %        | $m \pm s$ (ms) | %         | $m \pm s$ (ms) | %        | $m \pm s$ (ms) | %         | $m \pm s$ (ms) | %        | $m \pm s$ (ms) | %         | $m \pm s$ (ms) | %        | $m \pm s$ (ms) |
| WT     | 83         | 3.9±7.6        | 5        | -2.7±17        | 5         | -0.5±37        | 7        | -42±72         | 77        | -0.8±12        | 8        | 5.8±16         | 5         | -0.6±57        | 10       | -14±46         |
| LPD    | 85         | -2.7±7.4       | 2        | 40±13          | 1         | -7±35          | 12       | -48±63         | 63        | -2.4±13        | 9        | 32±20          | 6         | 4±67           | 22       | 54±60          |
| TU [7] | 82         | 4.2±8.6        | 8        | 36±15          | 4         | 9.6±38         | 6        | 32±40          | 72        | 7±16           | 16       | 31±18          | 4         | 9±35           | 8        | 49±45          |

TABLE VI  
DELINEATION RESULTS COMPARISON IN THE CSEDB. (N/R: NOT REPORTED; N/A: NOT APPLICABLE; #: NUMBER OF ANNOTATIONS)

| Method   | $P_{on}$<br>(#) $m \pm s$ (ms) | $P_{end}$<br>(#) $m \pm s$ (ms) | $QRS_{on}$<br>(#) $m \pm s$ (ms) | $QRS_{end}$<br>(#) $m \pm s$ (ms) | $T_{end}$<br>(#) $m \pm s$ (ms) |
|--|--------------------------------|---------------------------------|----------------------------------|-----------------------------------|---------------------------------|
| WT with multilead rule (this work)             | (25) -4.9±5.4                  | (24) -1.0±6.4                   | (32) 1.3±6.3                     | (27) 5.8±10.9                     | (26) 1.3±21.8                   |
| Laguna <i>et al</i> [16]                       | (30) 1.0±7.9                   | (29)-1.0±5.1                    | (30) -2.1±7.4                    | (25)-0.2±3.6                      | (26) 2.6±10.5                   |
| de Chazal <i>et al</i> [11]                    | N/A                            | N/A                             | (32) 0.9±3.6                     | (27) -0.6±7.1                     | N/A                             |
| Sahambi <i>et al</i> [20]                      | (N/R) N/R±4.0                  | (N/R) N/R±6.0                   | (N/R) N/R±2.0                    | (N/R) N/R±4.0                     | (N/R) N/R±20.0                  |
| <b>Tolerances (<math>2s_{CSE}</math>) [48]</b> | <b>10.2</b>                    | <b>12.7</b>                     | <b>6.5</b>                       | <b>11.6</b>                       | <b>30.6</b>                     |

referees is lower or similar to the error between cardiologists in all points, excepting an appreciable bias in the T end, which is insignificant when we take into account the whole database. To have a more reliable validation, it would be beneficial to have annotations of more than one cardiologist in the whole QTDB.

Regarding Table V, the stratification of the records according to the error is quite similar for all three methods in the case of the T peak, but the WT approach gives the largest percentage (around 77%) of well-detected recordings in the T wave end. In this group, the mean error was negligible while the standard deviation of the error in T end determination reduces to three samples (12 ms).

The CSEDB manual annotations were performed with information from all leads, while the presented WT-based delineator works on a single-channel basis. We observed that the multilead delineation performance was extraordinarily sensitive to the chosen parameters of the multichannel rule. In Table VI, we attained clearly worse results than those reported in [16] for QRS end and T end, with slight differences in the other points. Sahambi *et al.* reported in [20] lower error standard deviation in the CSE, especially in the QRS limits, although we have no information about what data set and what one-lead to multilead rule were used. As for the admitted tolerances, the “loose criteria” were accomplished by our delineation system. The “strict criteria” were only essentially accomplished in the P wave limits. Anyway, the significance of these results is limited by the reduced number of beats ( $\leq 32$ ), and by the great dependence on the multilead approach.

Finally, the results in the referee-reviewed automatic QRS onset annotations of the EDB allowed to validate the delineation in an extensive collection of beats ( $> 790\,000$ ). Using such a large data set, the bias was negligible, and the standard deviation of the error was around two sampling intervals.

In addition to the previously discussed features, the presented method can detect and delineate the individual waves of the QRS complex. However, we were not able to assess its perfor-

mance due to the lack of a conveniently annotated database for that kind of validation.

## V. CONCLUSION

We have presented and validated in this paper a wavelet-based ECG delineation system which performs QRS detection and provides as well the locations of the peak(s) of P, Q, R, S, R', and T waves, and the P, QRS, and T wave boundaries using a single analysis stage: the dyadic wavelet transform of the ECG signal. The algorithm has been validated using several standard annotated databases, with different sampling rates and a wide diversity of morphologies, making a total of more than 980 000 beats for QRS detection, more than 790 000 beats for QRS onset and more than 3500 beats other significant points.

The results have been compared with those of other published approaches and have shown that the developed algorithm provides a reliable and accurate delineation of the ECG signal, outperforming other algorithms, and with errors well within the observed intercardiologist variations. The most significant improvement was found in the T wave end, which shows, in general, the greatest difficulty in its determination, which is reflected in the largest intercardiologist differences. The clue for this performance improvement is, according to our understanding, the multiscale approach, which permits to attenuate noise at rough scales, and then to refine the precision of the positions with the help of finer scales.

While the assessment of QRS detectors can be reasonably and reliably done with the existing standard databases, we found difficulties for the evaluation of one-lead delineation algorithms. The number of annotated beats is still insufficient to have a good representation of the possible morphologies found in ECG signals. Additionally, there is not, to our knowledge, any available database with “single-lead annotations”, which would allow a more effective assessment and comparison of single-lead delineation algorithms.

## APPENDIX

The amplitude thresholds in the presented algorithms can be grouped into three types.

First, the thresholds used to decide if a pair of maximum moduli with opposite sign can account for a wave:  $\epsilon_{QRS}^1, \epsilon_{QRS}^2, \epsilon_{QRS}^3, \epsilon_{QRS}^4$  (for QRS detection),  $\epsilon_T$  and  $\epsilon_P$  (in T/P wave delineation). These thresholds are proportional to the RMS value of the WT at the corresponding scales. For QRS detection, in each excerpt of  $2^{16}$  samples

$$\epsilon_{QRS}^i = \text{RMS}(W_{2^i}x[n]), \quad i = 1, 2, 3 \quad (\text{A.1})$$

$$\epsilon_{QRS}^4 = 0.5 \text{RMS}(W_{2^4}x[n]). \quad (\text{A.2})$$

For T and P waves

$$\epsilon_T = 0.25 \text{RMS}(W_{2^4}x[n]) \quad (\text{A.3})$$

$$\epsilon_P = 0.02 \text{RMS}(W_{2^4}x[n]) \quad (\text{A.4})$$

where the RMS is measured in each interval between two consecutive QRS.

The morphology of QRS complexes and the type of T/P waves depend of the number of significant maximum moduli. The thresholds to determine if they are significant,  $\gamma_{QRS\_pre}, \gamma_{QRS\_post}, \gamma_T$ , and  $\gamma_P$  are related to the amplitude of the global maximum modulus within the corresponding search window (sw)

$$\gamma_{QRS\_pre} = 0.06 \max(|W_{2^2}x[n]|), \quad n \in \text{sw}_{QRS} \quad (\text{A.5})$$

$$\gamma_{QRS\_post} = 0.09 \max(|W_{2^2}x[n]|), \quad n \in \text{sw}_{QRS} \quad (\text{A.6})$$

$$\gamma_T = 0.125 \max(|W_{2^4}x[n]|), \quad n \in \text{sw}_T \quad (\text{A.7})$$

$$\gamma_P = 0.125 \max(|W_{2^4}x[n]|), \quad n \in \text{sw}_P. \quad (\text{A.8})$$

A third group of thresholds are used to determine the onset/end of QRS complex, T and P waves. They are proportional to the amplitude of the WT at the first/last maximum modulus of the complex or wave

$$\xi_{QRSon} = \begin{cases} 0.05 W_{2^2}x[n_{\text{first}}], & \text{if } W_{2^2}x[n_{\text{first}}] > 0 \\ 0.07 W_{2^2}x[n_{\text{first}}], & \text{if } W_{2^2}x[n_{\text{first}}] < 0 \end{cases} \quad (\text{A.9})$$

$$\xi_{QRSend} = \begin{cases} 0.125 W_{2^2}x[n_{\text{last}}], & \text{if } W_{2^2}x[n_{\text{last}}] > 0 \\ 0.71 W_{2^2}x[n_{\text{last}}], & \text{if } W_{2^2}x[n_{\text{last}}] < 0 \end{cases} \quad (\text{A.10})$$

$$\xi_{Ton} = 0.25 W_{2^4}x[n_{\text{first}}] \quad (\text{A.11})$$

$$\xi_{Tend} = 0.4 W_{2^4}x[n_{\text{last}}] \quad (\text{A.12})$$

$$\xi_{Pon} = 0.5 W_{2^4}x[n_{\text{first}}] \quad (\text{A.13})$$

$$\xi_{Pend} = 0.9 W_{2^4}x[n_{\text{last}}]. \quad (\text{A.14})$$

## REFERENCES

- [1] B.-U. Köhler, C. Hennig, and R. Orglmeister, "The principles of software QRS detection," *IEEE Eng. Med. Biol. Mag.*, vol. 21, pp. 42–57, Jan./Feb. 2002.
- [2] O. Pahlm and L. Sörnmo, "Software QRS detection in ambulatory monitoring – A review," *Med. Biol. Eng. Comp.*, vol. 22, pp. 289–297, 1984.
- [3] F. Grizali, "Toward a generalized scheme for QRS detection in ECG waveforms," *Signal Processing*, vol. 15, pp. 183–192, 1988.
- [4] G. M. Friesen *et al.*, "A comparison of the noise sensitivity of nine QRS detection algorithms," *IEEE Trans. Biomed. Eng.*, vol. 37, pp. 85–98, Jan. 1990.
- [5] L. Sörnmo, "A model-based approach to QRS delineation," *Comput. Biomed. Res.*, vol. 20, pp. 526–542, 1987.
- [6] I. Murthy and G. D. Prasad, "Analysis of ECG from pole-zero models," *IEEE Trans. Biomed. Eng.*, vol. 39, pp. 741–751, July 1992.
- [7] J. Vila, Y. Gang, J. Presedo, M. Fernandez-Delgado, and M. Malik, "A new approach for TU complex characterization," *IEEE Trans. Biomed. Eng.*, vol. 47, pp. 764–772, June 2000.
- [8] M. Nygard and L. Sörnmo, "Delineation of the QRS complex using the envelope of the ECG," *Med. Biol. Eng. Comput.*, vol. 21, pp. 538–547, Mar. 1983.
- [9] A. S. M. Koeleman, H. H. Ros, and T. J. van den Akker, "Beat-to-beat interval measurement in the electrocardiogram," *Med. Biol. Eng. Comput.*, vol. 23, pp. 213–219, 1985.
- [10] A. Algra and H. L. B. C. Zeelenberg, "An algorithm for computer measurement of QT intervals in the 24 hour ECG," in *Computers in Cardiology*. Los Alamitos, CA: IEEE Computer Society Press, 1987, pp. 117–119.
- [11] P. de Chazal and B. Celler, "Automatic measurement of the QRS onset and offset in individual ECG leads," presented at the *18th Ann. Int. Conf. IEEE Eng. Med. Biol. Soc.*, Amsterdam, The Netherlands, 1996.
- [12] I. K. Daskalov, I. A. Dotsinsky, and I. I. Christov, "Developments in ECG acquisition, preprocessing, parameter measurement and recording," *IEEE Eng. Med. Mag.*, vol. 17, pp. 50–58, 1998.
- [13] I. Daskalov and I. Christov, "Electrocardiogram signal preprocessing for automatic detection of QRS boundaries," *Med. Eng. Phys.*, no. 21, pp. 37–44, 1999.
- [14] —, "Automatic detection of the electrocardiogram T-wave end," *Med. Biol. Eng. Comput.*, vol. 37, pp. 348–353, 1999.
- [15] J. G. C. Kemmelings, A. C. Linnenbank, S. L. C. Muilwijk, A. Sippens-Groenewegen, A. Peper, and C. A. Grimbergen, "Automatic QRS onset and offset detection for body surface QRS integral mapping of ventricular tachycardia," *IEEE Trans. Biomed. Eng.*, vol. 41, pp. 830–836, Sept. 1994.
- [16] P. Laguna, R. Jané, and P. Caminal, "Automatic detection of wave boundaries in multilead ECG signals: Validation with the CSE database," *Comput. Biomed. Res.*, vol. 27, no. 1, pp. 45–60, Feb. 1994.
- [17] G. Speranza, G. Nollo, F. Ravelli, and R. Antolini, "Beat-to-beat measurement and analysis of the R-T interval in 24 h ECG Holter recordings," *Med. Biol. Eng. Comput.*, vol. 31, no. 5, pp. 487–494, Sept. 1993.
- [18] S. Meij, P. Klootwijk, J. Arends, and J. Roelandt, "An algorithm for automatic beat-to-beat measurement of the QT-interval," in *Computers in Cardiology*: IEEE Computer Society Press, 1994, pp. 597–600.
- [19] C. Li, C. Zheng, and C. Tai, "Detection of ECG characteristic points using wavelet transforms," *IEEE Trans. Biomed. Eng.*, vol. 42, pp. 21–28, Jan. 1995.
- [20] J. S. Sahambi, S. Tandon, and R. K. P. Bhatt, "Using wavelet transform for ECG characterization," *IEEE Eng. Med. Biol.*, vol. 16, no. 1, pp. 77–83, 1997.
- [21] M. Bahoura, M. Hassani, and M. Hubin, "DSP implementation of wavelet transform for real time ECG wave forms detection and heart rate analysis," *Comput. Meth. Programs Biomed.*, no. 52, pp. 35–44, 1997.
- [22] P. Strumillo, "Nested median filtering for detecting T-wave offset in ECGs," *Electron. Lett.*, vol. 38, no. 14, pp. 682–683, July 2002.
- [23] E. Soria-Olivas, M. Martínez-Sober, J. Calpe-Maravilla, J. F. Guerrero-Martínez, J. Chorro-Gascó, and J. Espí-López, "Application of adaptive signal processing for determining the limits of P and T waves in an ECG," *IEEE Trans. Biomed. Eng.*, vol. 45, pp. 1077–1080, Aug. 1998.
- [24] H. Vullings, M. Verhaegen, and H. Verbruggen, "Automated ECG segmentation with dynamic time warping," in *Proc. 20th Ann. Int. Conf. IEEE Engineering in Medicine and Biology Soc.*, Hong Kong, 1998, pp. 163–166.
- [25] Z. Dokur, T. Olmez, E. Yazgan, and O. Ersoy, "Detection of ECG waveforms by neural networks," *Med. Eng. Phys.*, vol. 19, no. 8, pp. 738–741, 1997.
- [26] W. Bystricky and A. Safer, "Modelling T-end in Holter ECG's by 2-layer perceptrons," in *Proc. Computers in Cardiology*. Los Alamitos, CA: IEEE Computer Society Press, 2002, vol. 29, pp. 105–108.
- [27] L. Clavier, J.-M. Boucher, R. Lepage, J.-J. Blanc, and J.-C. Cornily, "Automatic P-wave analysis of patients prone to atrial fibrillation," *Med. Biol. Eng. Comp.*, vol. 40, no. 1, pp. 63–71, Jan. 2002.
- [28] G. B. Moody and R. G. Mark, "The MIT-BIH arrhythmia database on CD-ROM and software for use with it," in *Computers in Cardiology*. Los Alamitos, CA: IEEE Computer Society Press, 1990, pp. 185–188.
- [29] P. Laguna, R. Mark, A. Goldberger, and G. Moody, "A database for evaluation of algorithms for measurement of QT and other waveform intervals in the ECG," in *Computers in Cardiology 1997*. Los Alamitos, CA: IEEE Computer Society Press, 1997, pp. 673–676.

- [30] A. Taddei, G. Distanti, M. Emdin, P. Pisani, G. B. Moody, C. Zeelenberg, and C. Marchesi, "The European ST-T database: Standards for evaluating systems for the analysis of ST-T changes in ambulatory electrocardiography," *Eur. Heart J.*, vol. 13, pp. 1164–1172, 1992.
- [31] J. L. Willems *et al.*, "A reference data base for multilead electrocardiographic computer measurement programs," *J. Amer. Coll. Cardiol.*, vol. 10, no. 6, pp. 1313–1321, 1987.
- [32] J. P. Martínez, S. Olmos, and P. Laguna, "Evaluation of a wavelet-based ecg waveform detector on the qt database," in *Computers in Cardiology*. Los Alamitos, CA: IEEE Computer Society Press, 2000, pp. 81–84.
- [33] S. Mallat and S. Zhong, "Characterization of signals from multiscale edge," *IEEE Trans. Pattern Anal. Machine Intell.*, vol. 14, pp. 710–732, July 1992.
- [34] J. S. Sahambi, S. Tandon, and R. K. P. Bhatt, "Wavelet based ST-segment analysis," *Med. Biol. Eng. Comput.*, vol. 36, no. 9, pp. 568–572, Sept. 1998.
- [35] S. Mallat, "Multifrequency channel decompositions of images and wavelet models," *IEEE Trans. Acoust. Signal Processing*, vol. 37, pp. 2091–2110, Dec. 1989.
- [36] A. Cohen and J. Kovačević, "Wavelets: The mathematical background," *Proc. IEEE*, vol. 84, pp. 514–522, Apr. 1996.
- [37] M. Akay, *Detecton and Estimation Methods for Biomedical Signals*. San Diego, CA: Academic, 1996.
- [38] N. V. Thakor, J. G. Webster, and W. J. Tompkins, "Estimation of QRS complex power spectrum for design of a QRS filter," *IEEE Trans. Biomed. Eng.*, vol. BME-31, pp. 702–706, Nov. 1984.
- [39] G. B. Moody and R. G. Mark, "Development and evaluation of a 2-lead ECG analysis program," in *Computers in Cardiology*. Los Alamitos, CA: IEEE Computer Society Press, 1982, pp. 39–44.
- [40] V. X. Afonso, W. J. Tompkins, T. Q. Nguyen, and S. Luo, "ECG beat detection using filter banks," *IEEE Trans. Biomed. Eng.*, vol. 46, pp. 192–201, Feb. 1999.
- [41] J. Lee, K. Jeong, J. Yoon, and M. Lee, "A simple real-time QRS detection algorithm," in *Proc. 18th Ann. Int. Conf. IEEE Engineering in Medicine and Biology Soc.*, 1996, pp. 1396–1398.
- [42] P. S. Hamilton and W. Tompkins, "Quantitative investigation of QRS detection rules using the MIT/BIH arrhythmia database," *IEEE Trans. Biomed. Eng.*, vol. BME-33, pp. 1157–1165, Dec. 1986.
- [43] J. Pan and W. J. Tompkins, "A real-time QRS detection algorithm," *IEEE Trans. Biomed. Eng.*, vol. BME-32, pp. 230–236, Mar. 1985.
- [44] R. Poli, S. Cagnoni, and G. Valli, "Genetic design of optimum linear and nonlinear QRS detectors," *IEEE Trans. Biomed. Eng.*, vol. 42, pp. 1137–1141, Nov. 1995.
- [45] J. Moraes, M. Freitas, F. Vilani, and E. Costa, "A QRS complex detection algorithm using electrocardiogram leads," in *Computers in Cardiology*. Los Alamitos, CA, 2002, vol. 29, pp. 205–208.
- [46] P. Hamilton, "Open source ECG analysis," in *Computers in Cardiology*. Los Alamitos, CA: IEEE Computer Society Press, 2002, vol. 29, pp. 101–104.
- [47] R. Jane, A. Blasi, J. García, and P. Laguna, "Evaluation of an automatic detector of waveforms limits in holer ECG with the QT database," in *Computers in Cardiology*. Los Alamitos, CA: IEEE Computer Society Press, 1997, pp. 295–298.
- [48] "Recommendations for measurement standards in quantitative electrocardiography," in *Eur. Heart J.*: The CSE Working Party, 1985, vol. 6, pp. 815–825.



**Juan Pablo Martínez** was born in Zaragoza, Aragon, Spain, in 1976. He received the M.Sc. degree in telecommunication engineering (with highest honors) from the University of Zaragoza (UZ), in 1999.

From 1999 to 2000, he was with the Department of Electronic Engineering and Communications, UZ, as a Research Fellow. Since 2000, he is an Assistant Professor in the same department. He is also involved as Researcher with the Aragon Institute of Engineering Research (I3A), UZ. His professional research activity lies in the field of biomedical signal processing, with main interest in signals of cardiovascular origin.

search activity lies in the field of biomedical signal processing, with main interest in signals of cardiovascular origin.



**Rute Almeida** was born in Porto, Portugal, in 1979. She received a 4-year degree in mathematics applied to technology from the Faculty of Sciences, University of Porto (FCUP), in 2000. Since October 2001, she is working towards the Ph.D. degree in the Applied Mathematics Department at FCUP, supported by a grant from Foundation for Science and Technology (Portugal) and European Social Fund.

She was with the Autonomic Function Study Center from Hospital S. João between March and October 2000, working in methods for automatic delineation of the ECG. Her main research interests are in time-scale methods and the automatic analysis of the ECG; namely, the study of ventricular repolarization.



**Salvador Olmos** (A'01–M'03) was born in Valencia, Spain, in 1969. He received the Industrial Engineering degree and the Ph.D. degree from the Polytechnic University of Catalonia, Catalonia, Spain, in 1993 and 1998, respectively.

He is currently an Associate Professor of Signal Processing and Communications in the Department of Electronics Engineering and Communications at Zaragoza University, Zaragoza, Spain. From August 2000 to August 2001, he was with the Department of Electrosience, Lund University, Lund, Sweden, supported by a post-doctoral research grant from Spanish Government. His professional research interests are in signal processing of biomedical signals.



**Ana Paula Rocha** was born in Coimbra, Portugal, in 1957. She received the Applied Mathematics degree and the Ph.D. degree in applied mathematics, systems theory and signal processing, from the Faculty of Sciences, University of Porto (FCUP), Porto, Portugal, in 1980 and 1993, respectively.

She is currently an Auxiliar Professor in the Department of Applied Mathematics at FCUP. Her research interests are in biomedical signals and system analysis (EMG, cardiovascular systems analysis, and autonomic nervous system characterization), time-frequency/time-scale signal analysis, point processes spectral analysis, and data treatment and interpretation.



**Pablo Laguna** (M'02) was born in Jaca, Spain, in 1962. He received the M.S. degree in physics and the Ph.D. degree from the University of Zaragoza (UZ), Zaragoza, Spain, in 1985 and 1990, respectively. The Ph.D. degree dissertation was developed at the Biomedical Engineering Division of the Institute of Cybernetics (IC), Polytechnic University of Catalonia (UPC-CSIC), Barcelona, Spain.

He is currently an Associate Professor in the Department of Electronic Engineering and Communications, UZ, and researcher in the Aragon Institute of Engineering Research (I3A), UZ. From 1987 to 1992, he worked as Assistant Professor in the Department of Control Engineering at the Politecnia University of Catalonia, Barcelona, Spain and as a Researcher at the Biomedical Engineering Division of the Institute of Cybernetics. His professional research interests are in Signal Processing, in particular applied to biomedical applications.